Analysis of terahertz pulses from large-aperture biased semi-insulating and arsenic-ion-implanted GaAs antennas

Rone-Hwa Chou, Tze-An Liu, and Ci-Ling Pan

Citation: Journal of Applied Physics **104**, 053121 (2008); doi: 10.1063/1.2967716
View online: http://dx.doi.org/10.1063/1.2967716
View Table of Contents: http://scitation.aip.org/content/aip/journal/jap/104/5?ver=pdfcov
Published by the AIP Publishing

Analysis of terahertz pulses from large-aperture biased semi-insulating and arsenic-ion-implanted GaAs antennas

Rone-Hwa Chou,[1,a)] Tze-An Liu,[2,b)] and Ci-Ling Pan[1,c)]
[1]*Department of Photonics and Institute of Electro-Optical Engineering, National Chiao Tung University, 1001 Ta Hsueh Road, Hsinchu, Taiwan 30010, Republic of China*
[2]*Center for Measurement Standards, Industrial Technology Research Institute, 321, Sec. 2, Kuang Fu Rd. Hsinchu, Taiwan 300, Republic of China*

(Received 17 March 2008; accepted 11 June 2008; published online 15 September 2008)

We investigate the characteristics of terahertz radiation pulses generated using biased semi-insulating and arsenic-ion-implanted GaAs photoconductive antennas with 1.5 cm aperture size under various pump fluences and bias fields. Compared with semi-insulating GaAs antenna, our arsenic-ion-implanted GaAs antenna exhibits larger bandwidth and better emission efficiency. Our simulation verifies that the superior characteristics for the latter can be partly attributed to larger optical absorption in the ion-implanted layer. For both types of antennas, we observe that the radiated peak terahertz amplitude displays an anomalous dependence on pump fluence, which deviates from the prediction given by the scaling rule. Analyzing the theoretical and simulation results, we infer that this behavior arises from band filling and two-photon absorption effects. At specific pump fluence, we find that the dependence of peak terahertz amplitude on bias field is distinct from the usual linear relationship predicted by the scaling rule. © *2008 American Institute of Physics*. [DOI: 10.1063/1.2967716]

I. INTRODUCTION

Terahertz radiation can be generated by employing femtosecond laser pulses to excite biased photoconductive (PC) antennas.[1] According to aperture size, a PC antenna with aperture size larger than 5 mm is classified as large aperture (or large area) types since its size is much larger than its radiation wavelength (approximately submillimeters). A typical configuration for a large-aperture biased antenna consists of two coplanar strip lines separated by 5 mm and above. Such an antenna can generate a giant terahertz radiation pulse with peak amplitude as high as 150 kV/cm when an expanded femtosecond laser beam is normally incident upon the antenna surface.[2] To increase terahertz emission efficiency, PC antennas with laterally structured emitter electrodes were employed.[3,4] Recently, Dreyhaupt *et al.*[5] reported a large-area PC terahertz emitter with an interdigitated electrode metal-semiconductor-metal structure and selective shadowing of optical excitation. Terahertz radiation with peak amplitude of 85 V/cm and bandwidth of about 2 THz were demonstrated by the use of a high bias field.[6,7] High terahertz field amplitude is desirable for potential applications for sensing, imaging,[8] telecommunications,[9,10] and nonlinear spectroscopy.[11] If the carrier lifetime τ_c of PC material for fabrication of a large-aperture antenna is much longer than the pump pulse duration τ_p, then the generated far-field terahertz pulse tends to exhibit a unipolar waveform, which is ideal for field ionization study.[12]

A significant criterion for assessing the performance of a biased PC antenna is its terahertz emission efficiency. In this regard, one can obtain insights by comparing the dependence of peak terahertz amplitude $E_r^{\max}$ on pump fluence F or bias field E_b.[13] $E_r^{\max}$ first grows rapidly with pump fluence for F below a characteristic fluence F_s, and then ascends slowly and linearly above F_s. This saturation behavior originates mainly from the near-field screening effect[14] that can be described by the scaling rule.[15] It was also shown that $E_r^{\max}$ scales linearly with E_b up to a breakdown value. In practice, either the F or E_b dependence will vary with different aperture sizes, pump spot sizes, or material properties.

Of all the PC materials studied, semi-insulating GaAs (SI-GaAs) and low-temperature-grown GaAs (LT-GaAs) were most widely used for terahertz emitters.[16] Some ion-implanted materials such as Fe-implanted InP ($InP:Fe^+$) (Ref. 17) or arsenic-ion-implanted GaAs ($GaAs:As^+$) have shown developments.[18,19] From a manufacturing viewpoint, the main benefit to the $GaAs:As^+$ antenna is that ion dosages can be accurately controlled during implantation. This advantage enables the $GaAs:As^+$ antenna to be reproducible in comparison with the LT-GaAs antenna, which has poor growth reliability. Therefore, recent works were devoted to studying whether the $GaAs:As^+$ antenna can become an alternative terahertz radiation source for the LT-GaAs antenna in terahertz radiation applications.

Implanting ions into SI materials will significantly change their original resistivity and temperature stability, as well as optical properties, such as τ_c or absorption coefficient α_0. The value of τ_c for As-implanted[20,21] or LT-GaAs antenna[22] is as short as 1 ps or less; hence, it influences terahertz radiation characteristics, including pulse shape, pulse duration, and bandwidth. Concerning the quantity α_0, its value is affected in the presence of impurity, bias field, or ion implantation. Nolte *et al.*[23] pointed out that LT-GaAs exhibits an excess absorption relative to GaAs, depending on

[a)]Electronic mail: ronehwa@hotmail.com.
[b)]Electronic mail: liutzean@itri.org.tw.
[c)]Electronic mail: clpan@faculty.nctu.edu.tw.

the growth conditions. On the other hand, Lin and Hsu[24] found that the band edge of absorption coefficient α_0 of GaAs:As^+ increases from 6.2×10^3 to 2.2×10^4 cm^{-1} for different dosages. Therefore, one can deduce that the absorption coefficient of SI materials tends to be altered after ion implantation.

Understanding the physics critical to the emission efficiency of terahertz antennas will allow greater control and wider applicability of terahertz radiation. Previously, Taylor and co-workers[25,26] used the current-surge model to explain several characteristics of large-aperture PC antennas, including terahertz pulse width, saturation, and pump wavelength dependence. In their model, the formation of terahertz pulses is associated with the carrier dynamics in PC material, and the time-dependent terahertz radiation is proportional to the time derivative of the surface photocurrent. We have investigated the optically excited terahertz radiation from PC dipole antennas with 5 μm gaps fabricated on SI-GaAs and multi-GaAs:As^+ antennas[19] and analyzed their characteristics by using the scaling rule. In the present paper, we will extend our previous work to large-aperture antennas. Additionally, we will analyze our experimental data by the use of the simulation results based on the formalism of nonlinear envelope and wave equations.

II. EXPERIMENTAL METHODS

Our basic experimental setup was a conventional terahertz time domain spectroscopy system.[27] In detail, we used a mode-locked regeneratively amplified Ti:sapphire laser (λ =800 nm) with 0.8 W average output power to generate pulses with duration τ_p of 50 fs at a 1 kHz repetition rate. The output laser beam was divided into a pump and a probe beam. The pump beam passed through a variable attenuator and was chopped at 200 Hz by a mechanical chopper. The probe power was fixed to ~30 mW. To overlap the whole antenna gap, the beam was first expanded by a concave lens with focal length of 5 cm, and then illuminates the gap at normal incidence. The terahertz radiation was generated by the laser excited, dc voltage applied large-aperture PC antenna fabricated on SI-GaAs and arsenic-ion-implanted GaAs (GaAs:As^+). The antenna is the AuGe/Ni/Au coated two strip line antenna with a gap spacing of 1.5 cm. The ion-implanted energy of GaAs:As^+ is 200 keV with postfurnace annealing of 600 °C for 30 min. The terahertz radiation was then emitted through the substrate, collimated by a pair of off-axis parabolic mirrors, and focused onto a ⟨110⟩-cut ZnTe crystal with 1 mm thickness. The other coherent probe laser was also transmitted through the crystal and resolved the terahertz field by a quarter wave plate, Wollaston prism, and balanced photodetectors. The terahertz waveform was mapped out by moving the delay line between the pump pulse and the probe pulse. The carrier lifetimes τ_c for both types of antennas were obtained from the optical pump-probe differential reflection measurement. In the pump fluence dependence experiment, pump fluence F was varied through a calibrated attenuator in front of the emitters.

III. THEORETICAL METHODOLOGY

In order to dedicate an explanation to the mechanisms underlying terahertz pulse waveforms, we adopt a methodology based on wave propagation scheme. If a pump pulse with field strength ξ propagates through a nonlinear dispersive medium (e.g., terahertz antenna) along the z direction, it will undergo several nonlinear effects, such as pulse dispersion β'', two-photon absorption α'', and optical-Kerr effect γ. The spatial z and time t dependent behavior associated with these phenomena is governed by the following nonlinear envelope equation for ξ:[28]

$$\left(\frac{\partial}{\partial z}+\frac{n_L}{c_0}\frac{\partial}{\partial t}\right)\xi=-\alpha(N_e)\xi-\alpha''|\xi|^2\xi+i\frac{\beta''}{2}\frac{\partial^2\xi}{\partial t^2}+i\gamma|\xi|^2\xi, \tag{1}$$

where

$$\alpha(N_e)=\alpha_0\left(\frac{N_{\max}-N_e}{N_{\max}}\right) \tag{2}$$

is the single-photon absorption caused by the band filling effect,[29] α_0 is the linear absorption coefficient, $N_{\max}$ is the population inversion threshold, N_e is the single-photon-excited electron concentration, while the constant n_L, c, and symbol i stand for linear refractive index, light vacuum speed, and imaginary unit, respectively. In Eq. (2), the evolutions of the N_e and single-photon-excited hole concentration N_h obey the current-continuity equations

$$\frac{\partial N_e}{\partial t}=\alpha(N_e)\frac{|\xi|^2}{2\eta h\nu\sqrt{\pi}}-\frac{N_e(x,z,t)}{\tau_c}, \tag{3}$$

$$\frac{\partial N_h}{\partial t}=\alpha(N_e)\frac{|\xi|^2}{2\eta h\nu\sqrt{\pi}}-\frac{N_h(x,z,t)}{\tau_c}, \tag{4}$$

where η denotes the medium impedance and $h\nu$ is the photon energy. The generated carriers are subjected to E_b and cause a conducting current J given by

$$J=J_e+J_h=q\{\mu_eN_e(x,z,t)+\mu_hN_h(x,z,t)\}E_b. \tag{5}$$

Here the quantities μ_e and μ_h denote the carrier mobilities for electron and hole, and q stands for the electron charge. Inside the medium, the current J induces an electromagnetic field E satisfying the second-order scalar wave equation

$$\nabla^2E-\mu\varepsilon\frac{\partial^2E}{\partial t^2}=\mu\frac{\partial J}{\partial t}. \tag{6}$$

In the far-field regime, evaluating the broadband Huygen–Fresnel diffraction integral[30] of E yields the far-field radiation field $E_r(t)$ as

$$E_r(t)=\int\frac{\cos(\hat{z},d')}{2\pi d'c_0}\frac{d}{dt}\left\{E\left(x',t-\frac{d}{c_0}\right)\right\}ds. \tag{7}$$

In this notation, $\hat{z}$ represents the unit vector in the z direction, the distance vector is denoted as d, and s refers to the differential area of the antenna's surface. The peak terahertz amplitude $E_r^{\max}$ can be obtained by evaluating the maximum of E_r.

TABLE I. Parameters used in terahertz radiation simulations for SI-GaAs and GaAs:As^+ antennas.

	α_0 (cm^{-1})	N_{max} (cm^{-3})	α'' (cm/GW)	n_L	μ_e , μ_h ($cm^2\ V^{-1}\ s^{-1}$)	β'' ($ps^2\ km^{-1}$)	γ (cm/GW)
SI-GaAs	6.5×10^3	2.0×10^{18}	286	3.4	1000, 50	120	3.2
GaAs:As^+	6.7×10^3	2.0×10^{18}	286	3.6	800, 20	120	3.2

In solving Eqs. (1) and (6), reflection boundary conditions are applied to ξ and E on the incident surface, while perfectly matched layer absorbing boundary conditions are assumed on the outer surface. For ξ, we assume a Gaussian function with duration of τ_p,

$$\xi(z,t=0)=\sqrt{\frac{2\eta F}{\tau_p}}\exp\left[-\frac{1}{2}\left(\frac{zn_L}{c_0\tau_p}\right)^2\right], \tag{8}$$

as an initial condition of Eq. (1). The values for the parameters included in Eqs. (1)–(8) are summarized in Table I.[28,29] To match the measured data, we select a lower N_{max} and higher α'' value than that reported in Ref. 28.

In the case of small-aperture antennas, the velocity overshoot, space-charge field screening, or photo-Dember[31] effects contribute to the formation of bipolar terahertz waveforms with bandwidth more than 1 THz, depending on F, E_b, and the incident condition of pump pulse. In our case, however, the measured waveforms reveal unipolar terahertz pulses with narrower bandwidth (~0.5 THz) rather than bipolar terahertz pulses with broader bandwidth at various F and normal incidence. This fact allows us to neglect the aforementioned three effects in our simulation for large-aperture antennas.

Although E_r^{max} can be obtained from Eq. (7) by evaluating the maximum of $E_r(t)$, as a comparison, we also present the E_r^{max} given by the scaling rule

$$E_r^{max}\approx D\frac{F/F_s}{1+F/F_s}, \tag{9}$$

where

$$D=\frac{An_L^{1/2}E_b}{4\pi\varepsilon_0c^2\eta_0\tau_d z} \tag{10}$$

and

$$F_s=\frac{(1+n_L)h\nu}{q(1-R)\mu_e\eta_0}. \tag{11}$$

IV. RESULTS AND DISCUSSIONS

A. Pump fluence dependence

1. Waveforms and spectra

In Fig. 1 we show the normalized photoreflectance changes $\Delta R/R$ with respect to the time delay t using SI-GaAs and GaAs:As^+ antennas. Fitting the data of Fig. 1 to exponential decays yields τ_c of 2.5 ps for the SI-GaAs antenna and 0.8 ps for the GaAs:As^+ antenna. Obviously, these τ_c values are much larger than the pump pulse duration τ_p(=0.05 ps). Here the values of τ_c are used to substitute into the calculation of Eqs. (7) and (8).

In Figs. 2(a) and 2(b), we present the measured terahertz radiation waveforms E_r from SI-GaAs and GaAs:As^+ antennas with E_b of 0.6 kV/cm under various pump fluences F. As can be seen, each waveform consists of a dominated peak followed by a relatively small and long negative tail. These waveforms can be characterized by four quantities: peak width dt (full width at half maximum), peak shift t_p, peak amplitude E_r^{max}, and minimum amplitude E_r^{min}. The normalized Fourier-transformed amplitude spectra $\tilde{E}_r$ of Figs. 2(a) and 2(b) are shown in Figs. 2(c) and 2(d). Due to the unipolar shapes in waveforms, the spectra contain small residual dc components that also can be seen from Ref. 5. For these spectra, we pay attention to their peak frequency f_p and frequency bandwidth df.

For the sake of comparison, we select one waveform individually from Figs. 2(a) and 2(b) at the same F and plot these two waveforms with normalization in Fig. 3(a). From Fig. 3(a) it was obtained that E_r^{min}=0.15 and dt=0.72 ps for the case of the SI-GaAs antenna, and E_r^{min}=0.08 and dt=0.70 ps for the case of the GaAs:As^+ antenna. The quantity dt is comparable to those observed in some centimeter-size antennas.[2] The Fourier-transformed amplitude spectra $\tilde{E}_r$ of Fig. 3(a) are plotted in Fig. 3(b). It was found that the quantity f_p for both types of antennas is equal to 0.13 THz, and the df (=0.57 THz) of GaAs:As^+ is larger than that in the case of SI-GaAs (df=0.52 THz).

With our aim being to explain the measured results of Figs. 3(a) and 3(b), we calculated Eqs. (1)–(8) by assuming that both α_0 and n_L of the GaAs:As^+ antenna are larger than those of the SI-GaAs antenna as seen in Table I. Figures 3(c) and 3(d) plot the simulated E_r and $\tilde{E}_r$ corresponding to Figs. 3(a) and 3(b). From Fig. 3(c), it was found that the simulated dt for SI-GaAs and GaAs:As^+ are 0.32 and 0.30 ps, respectively. Also, the simulated E_r^{min} is about 0.15, which is close to the measured one. In numerically studying the influence of the τ_c on E_r^{min}, we found that E_r^{min} is relevant to the values of the τ_c. The shorter the τ_c , the larger the E_r^{min}. Besides, the

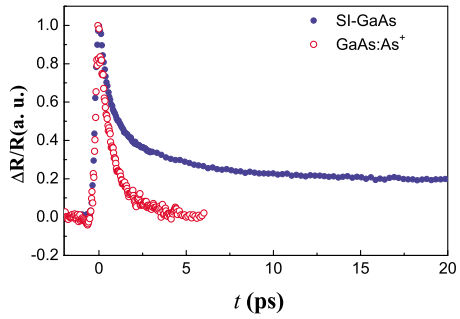

FIG. 1. (Color online) Transient normalized photoreflectance changes for SI-GaAs (solid blue circle) and GaAs:As^+ (open red circle) antennas.

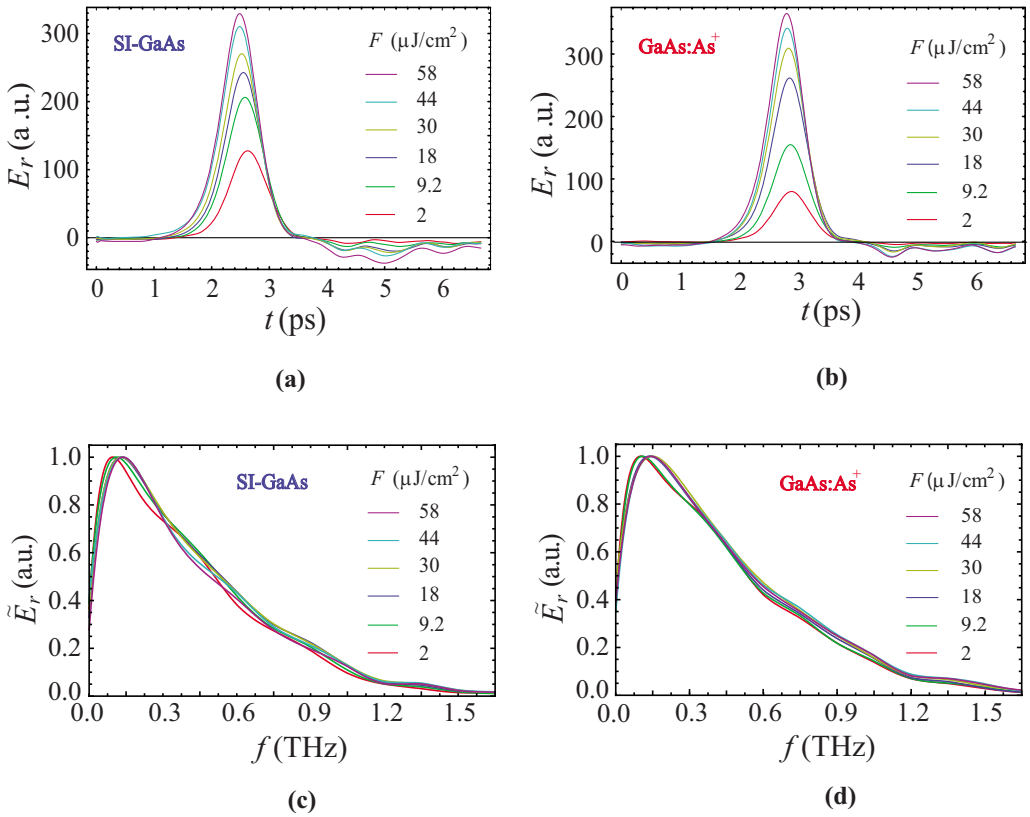

FIG. 2. (Color online) Measured terahertz waveforms E_r for (a) SI-GaAs and (b) GaAs:As$^+$ antennas as a function of time delay t at various pump fluences F. The bias field applied to the antennas was kept at 0.6 kV/cm. (c) Fourier-transformed amplitude spectrum $\tilde{E}_r$ of the waveforms in (a) and (d) $\tilde{E}_r$ of the waveforms in (b).

irregular negative waveforms stem from the pulse dispersion and optical-Kerr mechanism. In Fig. 3(d), the df of GaAs:As$^+$ reveals a larger value (df=1.5 THz) than that (df=1.2 THz) of SI-GaAs. This larger df of GaAs:As$^+$ merely reflects its shorter dt compared to the SI-GaAs case.

2. Peak width, peak shift, and bandwidth

Figure 4(a) plots the measured dt and t_p obtained from Figs. 2(a) and 2(b) as a function of F. It is remarkable that as

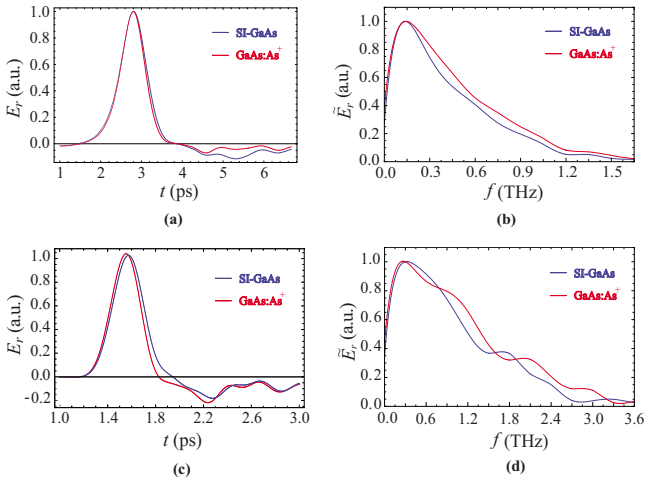

FIG. 3. (Color online) (a) Measured terahertz waveforms E_r, (b) corresponding Fourier-transformed amplitude spectrum $\tilde{E}_r$, and simulated (c) E_r and (d) $\tilde{E}_r$ for SI-GaAs (blue full line) and GaAs:As$^+$ (red full line) antennas at pump fluence F=58 μJ/cm^2. Both E_r and $\tilde{E}_r$ are normalized to their peak amplitude.

F increases from 2 to 58 μJ/cm^2, the quantity dt of SI-GaAs decreases monotonically to its minimal value located at the turning point (F=30 μJ/cm^2, dt=0.72 ps) and subsequently increases from that point onward. In the case of GaAs:As$^+$, dt varies with F in a manner similar to the case of SI-GaAs, but its turning point occurs at higher F(=44 μJ/cm^2) than that in the case of SI-GaAs. For both types of antennas, the quantity t_p reveals an increasing trend with the increase of F. Also, the dt or t_p value for GaAs:As$^+$ is less than that for SI-GaAs at each value of F. Although the measured dt values in Fig. 4(a) are close to those obtained by Hattori *et al.*,[5] it is worth noting that the phenomenon relevant to the turning point was not found in their experiments.

To interpret the measured results of Fig. 4(a), with the assumption of α_0 and n_L being the same as the case of Fig. 3(c), we calculated Eqs. (1)–(8) at different F and present the results in Fig. 4(b). As seen in this figure, the simulated data produced a monotonic decrease in dt and an increase in t_p with increasing F. In addition, the simulated dt or t_p for GaAs:As$^+$ is less than that for SI-GaAs, mainly due to a larger α_0 and n_L in GaAs:As$^+$. However, it was found that the turning point behavior does not appear in the simulated dt.

From the spectra in Figs. 2(c) and 2(d), we plotted the measured df and f_p in Fig. 4(c) as a function of F. Obviously, one can see from Fig. 4(c) that the df of GaAs:As$^+$ is larger than that of SI-GaAs under various F. This larger df for GaAs:As$^+$ reflects the shorter dt shown in Fig. 4(a). In

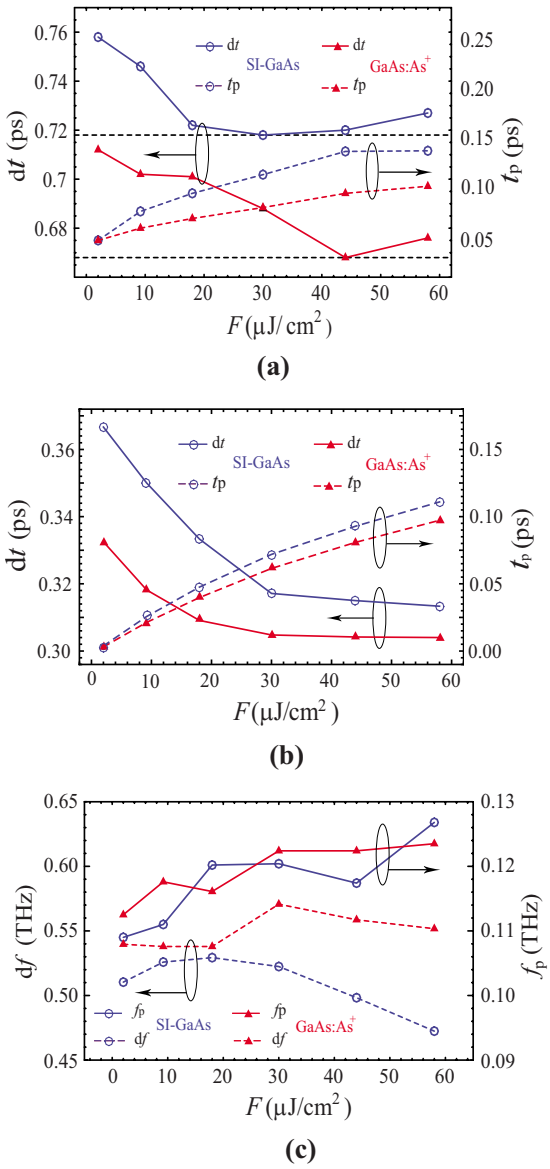

FIG. 4. (Color online) (a) Measured peak width dt (full line) and peak shift t_p (dashed line) obtained from Figs. 2(a) and 2(b), (b) simulated dt (full line) and t_p (dashed line), and (c) measured peak frequency f_p (full line) and bandwidth df (dashed line) obtained from Figs. 2(c) and 2(d) as a function of pump fluence F for both SI-GaAs (blue) and GaAs:As$^+$ (red) antennas.

addition, it can be perceived that f_p, as well as the difference between two df, has an increasing trend with the increase of F.

3. Peak terahertz amplitude

In Fig. 5(a) we show the measured $E_r^{\max}$ of SI-GaAs and GaAs:As$^+$ antennas as a function of pump fluence from $F=2$ up to 170 μJ/cm^2. We observe that as F increases from 2 to 58 μJ/cm^2, both $E_r^{\max}$ curves increase monotonically. Compared with the SI-GaAs case, the $E_r^{\max}$ values of the GaAs:As$^+$ antenna are lower, provided that $F<20$ μJ/cm^2, but exceed that of the SI-GaAs antenna, provided that $F>20$ μJ/cm^2; hence both curves intersect at $F=20$ μJ/cm^2. In addition, note that both curves reach their respective maxima in the vicinity of $F=60$ μJ/cm^2, then gradually become reduced instead of further increasing as F increases

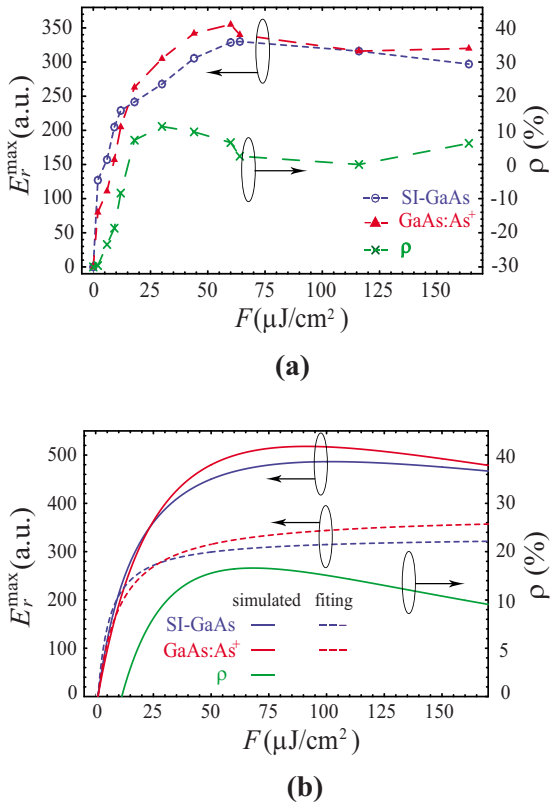

FIG. 5. (Color online) (a) Measured (dashed marks), (b) fitting (dashed line), and simulated (full line) terahertz peak amplitudes $E_r^{\max}$ vs pump fluence F for both SI-GaAs (blue) and GaAs:As$^+$ (red) antennas. The green dashed cross and full lines are the ratio $\rho\{\equiv[E_r^{\max}(\text{GaAs:As}^+)-E_r^{\max}(\text{SI-GaAs})]/E_r^{\max}(\text{SI-GaAs})\}$ for measured and simulated cases. The bias field E_b was kept at 0.6 kV/cm.

from 60 to 170 μJ/cm^2. We designate this phenomenon as anomalous saturation since the quantity in normal saturation tends to increase slowly with the increase of F rather than reducing to a lower value. From these two anomalous saturation data, it is instructive to gain insight into how the difference in $E_r^{\max}$ between two types of antennas varies with F. To quantify this difference, we introduce a relative emission efficiency ρ defined as the ratio of the difference in peak terahertz amplitude between two types of antennas to peak terahertz amplitude of the SI-GaAs antenna, that is, $\rho \equiv [E_r^{\max}(\text{GaAs:As}^+)-E_r^{\max}(\text{SI-GaAs})]/E_r^{\max}(\text{SI-GaAs})$. Figure 5(a) also shows the F dependence of the relative emission efficiency ρ in percentage term (%). In particular, it appears that the quantity ρ first grows from $F=2$ μJ/cm^2 until it reaches to a maximum ($\sim$12%) at $F=30$ μJ/cm^2 and finally reduces, tending to lower values for high enough F.

In contrast to our previous study (see Ref. 19), where we compared the emission efficiency of SI-GaAs and multi-GaAs:As$^+$ antennas with a gap size of 5 μm, our large-aperture GaAs:As$^+$ antenna takes advantage of better terahertz emission efficiency than our SI-GaAs one, above specific F. In Ref. 16, one can see that a similar advantage also happens to the dipole-I LT-GaAs small-aperture antenna, which exhibits better emission efficiency relative to the case of SI-GaAs, above a pump power of 21 mW. Nevertheless, its advantage has not been confirmed theoretically. On the other hand, although the anomalous saturation does not occur

at our previous GaAs:As^+ small-aperture antenna, it was observed by Tani *et al.*[16] in dipole-I SI-GaAs small-aperture antenna and also by Löffler *et al.*[32] and Hasegawa[33] in large-aperture SI-GaAs antenna. In Ref. 33, the anomalous saturation was attributed to the initial carrier effect.

In an attempt to theoretically reproduce the relation between the measured $E_r^{\max}$ and F, we fit our measured $E_r^{\max}$ using the scaling rule given by Eq. (9) and report the fitting results in Fig. 5(b). From these two fitting curves, it was obtained that $D=331.5$ and $F_s=5.3$ $\mu J/cm^2$ for SI-GaAs, and $D=377.6$ and $F_s=9.7$ $\mu J/cm^2$ for GaAs:As^+. Accordingly, either the F_s or D values in the GaAs:As^+ case are larger than those in the SI-GaAs case. Note that F_s depends on both the μ_e and n_L according to Eq. (11). Under the same pump wavelength, a larger F_s for GaAs:As^+ implies two consequences: one is that its μ_e value is lower than that of SI-GaAs since F_s is inversely proportional to μ_e; the other is that its n_L is larger than that of SI-GaAs since F_s is proportional to n_L. Both consequences are reasonable since ion implantation reduces the μ_e value, whereas increasing the α_0 value leads to the increase of n_L due to the reciprocal relationship between α_0 and n_L. Under the same pump and detection configuration, a larger D for GaAs:As^+ indicates that the quantity $n_L^{1/2}$ of GaAs:As^+ is also larger than that of SI-GaAs according to Eq. (10). Therefore, an increase in n_L leads to a higher D for GaAs:As^+ compared to SI-GaAs. In contrast to the measured $E_r^{\max}$ in Fig. 5(a), although the fitting curves in Fig. 5(b) are able to account for the $E_r^{\max}$ behavior at low F, it is still not consistent with the measured $E_r^{\max}$ at the high F regime. To resolve this discrepancy, we considered the band-filling and two-photon absorption effects as described in Sec. III instead of the initial carrier effect presented in Ref. 33. From the implication of the fitting curves given by the scaling rule, we evaluated Eqs. (1)–(8), provided that n_L for GaAs:As^+ is 1.06 times larger than that for SI-GaAs, and also plotted the two simulated $E_r^{\max}$ along with ρ in Fig. 5(b). As shown in the graph, each simulated $E_r^{\max}$ initially increases at increasing values of F, reaches a maximum at about $F=80$ $\mu J/cm^2$, and then starts decreasing gradually at large values of F. Similarly to the measured case, the $E_r^{\max}$ value of GaAs:As^+ is lower than that of SI-GaAs below $F=20$ $\mu J/cm^2$, but higher than $F=20$ $\mu J/cm^2$. Besides, the maximum of the simulated ρ (~16%) appears at about $F=55$ $\mu J/cm^2$.

Referring to the simulated dependency in Fig. 5(b), the trends in $E_r^{\max}$ and anomalous saturation behavior are both consistent with our experimental observation of Fig. 5(a). Accordingly, we infer that the GaAs:As^+ antenna possesses a larger refractive index n_L and smaller μ_e so that the $E_r^{\max}$ value for GaAs:As^+ is lower than that for SI-GaAs, below $F=20$ $\mu J/cm^2$, but higher than $F=20$ $\mu J/cm^2$. In another respect, in the region of pump fluence more than 60 $\mu J/cm^2$, the effects of band filling and two-photon absorption become obvious and confine the values of $E_r^{\max}$.

B. Bias dependence

We next examine the dependence of $E_r^{\max}$ on E_b at specific F where the emission efficiency of GaAs:As^+ is higher than that of SI-GaAs. Figure 6 contains our results for the measured $E_r^{\max}$ of SI-GaAs and GaAs:As^+ antennas as a function of E_b at $F=58$ $\mu J/cm^2$. It clearly appears that the experimental data apparently fit the linear relationships from $E_b=0.5$ to 0.85 kV/cm for both types of antennas. Besides, the zero-intercept line for GaAs:As^+ has a larger slope than that for SI-GaAs, implying that GaAs:As^+ has a considerably higher $E_r^{\max}$ than does SI-GaAs at any same E_b value. These two linear trends are analogous to those found in other large-aperture antennas (see Refs. 14 and 15). As expected on the basis of the scaling rule, the origin of these linear dependences can be interpreted straightforwardly by the linear relation between $E_r^{\max}$ and E_b in accordance with Eqs. (9) and (10). In terahertz antenna literature, we do not find any exception deviating from this linear relation.

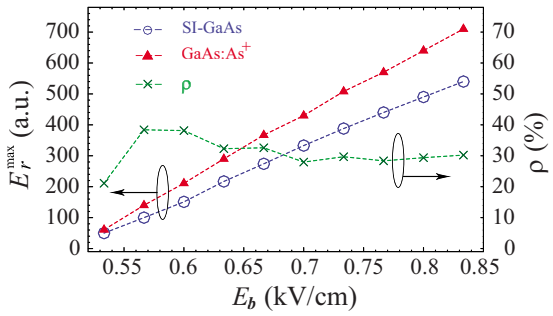

FIG. 6. (Color online) Measured peak terahertz amplitude $E_r^{\max}$ from SI-GaAs (blue dashed circle) and GaAs:As^+ (red dashed triangle) antennas and the relative emission efficiency ρ (green dashed cross) as a function of bias field E_b at pump fluence $F=58$ $\mu J/cm^2$.

Also shown in Fig. 6 is the relative emission efficiency ρ. Remarkably, ρ first grows until it reaches its maximum (~40%) in the vicinity of 0.57 kV/cm, then subsequently reduces to 30%, and does not decrease anymore at the high E_b regime. To the best of our knowledge, this special characteristic has not been discovered by any group except ours. Its importance lies in the fact that if the two zero-intercept lines in Fig. 6 were exactly linear, the values in ρ would supposedly form a horizontal line rather than a curve. Accordingly, we infer that the relationships between $E_r^{\max}$ and E_b are not exactly linear for our or even other group's cases. In other words, the scaling rule expressed by Eq. (9) is not a rigorous model, and the mechanism responsible for the maximum of ρ at low E_b regime is due to a nonlinear relationship between $E_r^{\max}$ and E_b. Nevertheless, its exact theoretical relationship remains unknown to us.

V. CONCLUSIONS

We have performed a comparative study between terahertz radiation waveforms for large-aperture biased SI-GaAs and GaAs:As^+ antennas under various pump fluences and bias field. The terahertz pulses emitted from our GaAs:As^+ antenna have narrower peak width, wider bandwidth, and higher peak terahertz amplitude than those obtained from the SI-GaAs antenna. The peak frequency and bandwidth difference between these two types of antennas have increasing trends with increasing pump fluence. From the pump fluence dependence of peak terahertz amplitude, we have found that

SI-GaAs and GaAs:As^+ antennas both exhibit anomalous saturation behaviors, which can be reproduced numerically by incorporating nonlinear effects into a rigorous electromagnetic wave propagation model. Above a pump fluence of 20 $\mu J/cm^2$, the GaAs:As^+ antenna obtained better emission efficiency relative to the SI-GaAs antenna. On the basis of numerical simulation, we have deduced that this better emission efficiency stems from the fact that both types of antennas have different quantities, including linear absorption coefficient, refractive index, and carrier mobility. For the GaAs:As^+ antenna, the first two quantities are larger, whereas the last is smaller in comparison with the SI-GaAs antenna. We have also inferred from our simulation that the band filling and two-photon absorption effects are responsible for the anomalous saturation behavior. In the bias field dependence of measured peak terahertz amplitude, we have found that the emission efficiency of the GaAs:As^+ antenna is higher than that of the SI-GaAs antenna and that the relative emission efficiency reaches maximum at specific bias field. This particular behavior convinces us that a more rigorous model is required for interpreting the bias field dependence of peak terahertz amplitude instead of the scaling rule, and we believe that it will be an important topic worthy of being investigated further.

ACKNOWLEDGMENTS

This work was partially supported by the Academic Top Universities Program of the Ministry of Education and various grants of the National Science Council of Taiwan, Republic of China.

[1]D. You, R. R. Jones, P. H. Bucksbaum, and D. R. Dykaar, Opt. Lett. **18**, 290 (1993).
[2]T. Hattori, K. Tukamoto, and H. Nakatsuka, Jpn. J. Appl. Phys., Part 1 **40**, 4907 (2001).
[3]S. R. Andrews, A. Armitage, P. G. Huggard, and A. Hussain, Phys. Med. Biol. **47**, 3705 (2002).
[4]G. Zhao, R. N. Schouten, N. van der Valk, W. T. Wenckebach, and P. C. M. Planken, Rev. Sci. Instrum. **73**, 1715 (2002).
[5]A. Dreyhaupt, S. Winnerl, T. Dekorsy, and M. Helm, Appl. Phys. Lett. **86**, 121114 (2005).
[6]D. A. Turton, G. H. Welsh, J. J. Carey, G. D. Reid, G. S. Beddard, and K. Wynne, Rev. Sci. Instrum. **77**, 083111 (2006).
[7]S. Winnerl, A. Dreyhaupt, F. Peter, D. Stehr, M. Helm, and T. Dekorsy, *Nonequilibrium Carrier Dynamics in Semiconductors* (Springer, Berlin, 2006), Vol. 110, p. 73.
[8]B. B. Hu and M. C. Nuss, Opt. Lett. **20**, 1716 (1995).
[9]T.-A. Liu, G.-R. Lin, Y.-C. Chang, and C.-L. Pan, Opt. Express **13**, 10416 (2005).
[10]S. Ramsey, E. Funk, and C. H. Lee, Technical Digest of the International Topical Meeting on Microwave Photonics '99, 1999 (unpublished), p. 265.
[11]R. R. Jones, D. You, and P. H. Bucksbaum, Phys. Rev. Lett. **70**, 1236 (1993).
[12]X. Zhang and R. R. Jones, Phys. Rev. A **73**, 035401 (2006).
[13]P. K. Benicewicz and A. J. Taylor, Opt. Lett. **18**, 1332 (1993).
[14]J. T. Darrow, X.-C. Zhang, D. H. Auston, and J. D. Morse, IEEE J. Quantum Electron. **28**, 1607 (1992).
[15]P. K. Benicewicz, J. P. Roberts, and A. J. Taylor, J. Opt. Soc. Am. B **11**, 2533 (1994).
[16]M. Tani, S. Matsuura, K. Sakai, and S. Nakashima, Appl. Opt. **36**, 7853 (1997).
[17]T.-A. Liu, M. Tani, M. Nakajima, M. Hangyo, K. Sakai, S. Nakashima, and C.-L. Pan, Opt. Express **12**, 2954 (2004).
[18]J. Lloyd-Hughes, E. Castro-Camus, M. D. Fraser, H. H. Tan, C. Jagadish, and M. B. Johnston, Phys. Rev. B **70**, 235330 (2004).
[19]T.-A. Liu, M. Tani, and C.-L. Pan, J. Appl. Phys. **93**, 2996 (2003).
[20]M. Tani, K. Sakai, H. Abe, S. Nakashima, H. Harima, M. Hangyo, Y. Tokuda, K. Kanamoto, Y. Abe, and N. Tsukada, Jpn. J. Appl. Phys., Part 1 **33**, 4807 (1994).
[21]S. Gupta, J. F. Whitaker, and G. A. Mourou, IEEE J. Quantum Electron. **28**, 2464 (1992).
[22]H.-H. Wang, P. Grenier, J. F. Whitaker, H. Fujioka, J. Jasinski, and Z. Liliental-Weber, IEEE J. Sel. Top. Quantum Electron. **2**, 630 (1996).
[23]D. D. Nolte, W. Walukiewicz, and E. E. Haller, Phys. Rev. Lett. **59**, 501 (1987).
[24]G.-R. Lin and C.-C. Hsu, J. Appl. Phys. **89**(11), 6536 (2001).
[25]A. J. Taylor, P. K. Benicewicz, and S. M. Young, Opt. Lett. **18**(16), 1340 (1993).
[26]G. Rodriguez, S. R. Caceres, and A. J. Taylor, Opt. Lett. **19**(23), 1994 (1994).
[27]Q. Chen and X.-C. Zhang, Appl. Phys. Lett. **74**, 3435 (1999).
[28]E. A. Bahaa and M. C. Teich, *Fundamentals of Photonics* (Wiley, New York, 1991), Chap. 19.
[29]F. Kadlec, H. Nemec, and P. Kuzel, Phys. Rev. B **70**, 125205 (2004).
[30]J. W. Goodman, *Introduction to Fourier Optics* (McGraw-Hill, New York, 1996).
[31]T. Dekorsy, H. Auer, H. J. Bakker, H. G. Roskos, and H. Kurz, Phys. Rev. B **53**, 4005 (1996).
[32]T. Löffler, T. Hahn, M. Thomson, F. Jacob, and H. G. Roskos, Opt. Express **13**, 5353 (2005).
[33]N. Hasegawa, Thesis, University of Frankfurt, 2004.